RESEARCH ARTICLE

Dielectric Hole Etching With C_2F_4O and C_2HF_3O as a Replacement of CF_4/O_2

Jun Won Jeong[1] | Jong Woo Hong[2] | Hyeong Joon Eoh[3] | Chan Ho Kim[3] | Kyung Lim Kim[4,5] | Sung Hyun Kim[2] | Young Woo Jeon[6] | Jong Soon Park[4,5] | Hyun Min Cho[7] | Yu Gwang Jeong[7] | Da Woon Jung[7] | Yun Jong Yeo[7] | Geun Young Yeom[2,3] | Dong Woo Kim[2]

[1]Department of Semiconductor Convergence Engineering, Sungkyunkwan University (SKKU), Suwon, Gyeonggi-do, Republic of Korea | [2]School of Advanced Materials Science and Engineering, Sungkyunkwan University (SKKU), Suwon, Gyeonggi-do, Republic of Korea | [3]SKKU Advanced Institute of Nanotechnology (SAINT), Sungkyunkwan University (SKKU), Suwon, Gyeonggi-do, Republic of Korea | [4]Department of Semiconductor and Display Engineering, Sungkyunkwan University (SKKU), Suwon, Gyeonggi-do, Republic of Korea | [5]Samsung Institute of Technology, Yongin-si, Gyeonggi-do, Republic of Korea | [6]Department of Display Engineering, Sungkyunkwan University (SKKU), Suwon, Gyeonggi-do, Republic of Korea | [7]Process Research Team, Yongin-si, Republic of Korea

Correspondence: Geun Young Yeom (gyyeom@skku.edu) | Dong Woo Kim (dwkim111@gmail.com)

Received: 12 June 2025 | **Revised:** 13 July 2025 | **Accepted:** 16 July 2025

Funding: This work was supported by Samsung Display Co. Ltd. (S-2024-1085-000-01) and the Technology Innovation Program Development Program-Development of core technology in Carbon Neutrality (RS-2023-00265858, Development of alternative PFC gas with low GWP value under 150 for OLED display oxide TFT insulator patterning) funded by the Ministry of Trade, Industry & Energy (MOTIE, Korea).

Keywords: C_2F_4O | C_2HF_3O | CF_4 | global warming potential | nitride | oxide | plasma etching

ABSTRACT

Advanced display technology requires enhanced etch characteristics such as smaller critical dimensions, higher etch selectivity over PR, and lower surface damage, etc. In addition, CF_4 has a high global warming potential. The results showed that, even though these alternative gasses exhibited slightly lower etch rates of ~80% and ~62% for C_2F_4O and C_2HF_3O, respectively, compared to CF_4/O_2, C_2F_4O showed similar etch characteristics compared to CF_4/O_2, and C_2HF_3O showed a higher etch selectivity over PR and a more anisotropic etch profile. When the total global warming potential (Million Metric Tons of Carbon Equivalent; MMTCE) was measured, the etching with C_2F_4O showed a reduction of ~45% and C_2HF_3O a reduction of approximately ~84% in MMTCE compared to CF_4/O_2.

1 | Introduction

Recently, low-temperature polycrystalline silicon (LTPS) technologies have been widely developed for display devices due to their higher electron mobility compared to other thin-film transistor (TFT) material technologies [1–5]. For the LTPS devices, a dielectric layer composed of SiN_x and SiO_x is used and, for the contact hole etching of the dielectric layer, fluorine containing gasses such as $CHF_3/O_2/Ar$, $SF_6/O_2/Ar$, $C_4F_8/O_2/Ar$, and, especially, $CF_4/O_2/Ar$ have been successfully used [6, 7]. However, the etch gasses used to etch the contact hole such as CF_4 (GWP = 7380), SF_6 (GWP = 25 200), CHF_3 (GWP = 14 600), and C_4F_8 (GWP = 8700) have high global warming potentials (GWPs) along with the low etch selectivity between the dielectric layer and photoresist (PR) [8].

Recent advancement of display technology toward higher resolutions require smaller and deeper holes while minimizing the critical dimension (CD) loss similar to semiconductor devices [9–11]. In addition, even with the importance of environmental, social, and governance (ESG) issues, perfluorocarbon (PFC) and

Jun Won Jeong and Jong Woo Hong contributed equally to this study.

© 2025 Wiley-VCH GmbH.

hydrofluorocarbon (HFC) emissions in the semiconductor and display industries have increased by more than 30% [12–16]. Therefore, addressing these issues through process optimization and the adoption of low GWP gasses for the etching is becoming increasingly critical [17, 18].

To resolve these issues, in display manufacturing, various fluorine-based gasses with low GWPs such as COF_2, HF/H_2, C_3F_6, and so forth have been studied in the etching of dielectric contact holes to replace high GWP etch gasses, especially to replace CF_4 gas [19–22]. The research was generally focused on etching of SiN_x or SiO_x only, and the continuous one-step etching of a dielectric layer composed of SiN_x or SiO_x using low GWP gasses has not been performed [23, 24]. Furthermore, in some cases, high GWP gasses tend to form through the recombination of dissociated gasses at the exhaust stage after etching using low GWP fluorocarbon based gases, and not many studies related to the recombination of dissociated low GWP gases can be found from the previous research, therefore, it is also important to analyze the total GWPs (Million Metric Tons of Carbon Equivalent; MMTCE) at the exhaust stage [16, 18, 20, 21].

This study is focused on the contact hole etching of the dielectric layer composed of SiN_x and SiO_x using inductively coupled plasma (ICP) with low GWP fluorocarbon gases for the formation of contact holes masked with PR. When replacing with low GWP alternative gases for the etching of various dielectric layers, the etch characteristics by using the low GWP gases should be similar to or better than those with the etch gases previously used [25, 26]. As the low GWP fluorocarbon gas replacing CF_4, trifluoro acetyl fluoride (C_2F_4O)/Ar has been investigated to achieve similar etch characteristics to the $CF_4/O_2/Ar$. Additionally, trifluoroacetaldehyde (C_2HF_3O) has also been investigated to improve the etch selectivity over PR and underlying layers while sacrificing the etch rates. The etch mechanisms were investigated using surface analysis methods such as X-ray photoelectron spectroscopy (XPS) and plasma analysis methods such as quadrupole mass spectrometry (QMS) and optical emission spectroscopy (OES). The formation of high-GWP gases at the exhaust line was also investigated with a Fourier transform infrared spectrometer (FT-IR) installed at the dry pump located at the exhaust stage.

2 | Experimental Details

The contact hole etching experiment was carried out in a 300 mm diameter ICP chamber. The 300 mm ICP system used in the experiment is shown in Figure 1a, and the PR-masked $SiN_x/SiO_x/SiN_x/SiO_x$ layer is presented in Figure 1b. The antenna of the ICP source consisted of two copper turn-two coils: inner and outer turn coils. A 35-mm-thick alumina window was placed over the top electrode for etching, and the 300 mm diameter substrate holder was made of anodized aluminum. The distance between the substrate and the electrode was approximately 15 cm. The radio frequency (RF) power to the ICP antenna was supplied by a 13.56 MHz RF generator (Seren-R3001), while the bias power to the substrate holder was provided by a 2 MHz RF generator (Seren-R2001). The process chamber was pumped by a 3000 L/s turbo pump and a dry pump, and the operating pressure was controlled by a pendulum valve (VAT-model PM.7). The substrate was cooled using a chiller and maintained at room temperature.

The dielectric layer composed of $SiN_x/SiO_x/SiN_x/SiO_x$ was deposited on amorphous silicon/glass substrates by plasma-enhanced chemical vapor deposition, and the thickness was 1335 nm. The dielectric layer composed of $SiN_x/SiO_x/SiN_x/SiO_x$ was masked with a 1736 nm thick positive PR, and the bottom CD width of the hole PR pattern was approximately 1800 nm. These structural parameters were selected based on typical feature sizes found in state-of-the-art OLED or LTPS display devices. The $SiN_x/SiO_x/SiN_x/SiO_x$ contact hole etching was conducted under consistent conditions for all three gases, with an ICP source power of 2000 W, DC voltage of −500 V, chamber pressure of 30 mTorr, and a substrate temperature of 18°C. When the process pressure was lower than 30 mTorr, significant CD loss occurred, while at pressures higher than 30 mTorr, severe micro-trenching was observed. When the bias voltage exceeded −500 V, sidewall damage was observed, whereas a weaker bias resulted in reduced selectivity over the mask. Ar was fixed to maintain plasma density and enhance ionization efficiency, while the flow rates of the alternative gasses were gradually adjusted during the experiments. For CF_4, the process was optimized using a gas mixture of CF_4 (30−110 sccm)/O_2 (5 sccm)/Ar (150 sccm). For the alternative

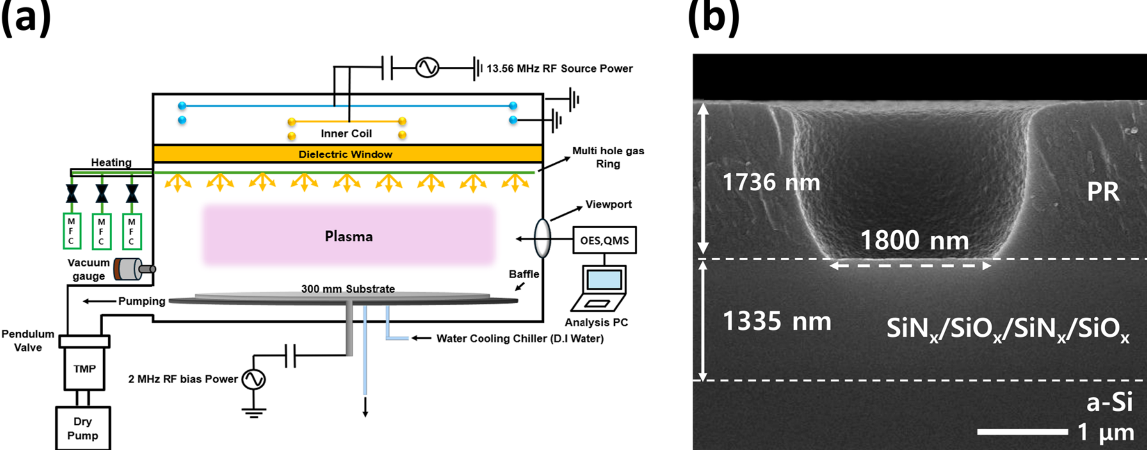

FIGURE 1 | (a) Schematic diagram of the 300 mm ICP used in the experiment. (b) SEM image of SiN_x/SiO_x reference structure masked by PR. PR height was 1736 nm, and mask hole CD was 1800 nm.

16128869, 2025, 10, Downloaded from https://onlinelibrary.wiley.com/doi/10.1002/ppap.70068 by Sungkyunkwan University, Wiley Online Library on [03/02/2026]. See the Terms and Conditions (https://onlinelibrary.wiley.com/terms-and-conditions) on Wiley Online Library for rules of use; OA articles are governed by the applicable Creative Commons License

TABLE 1 | Information on GWP of CF_4, C_2F_4O, C_2HF_3O, and CF_4O in addition to the gas name, molecular weight, and CAS number used in the experiment.

IUPAC name	Molecular formula	Molecular weight (g/mol)	GWP 100_{yr}	Cas number
Tetrafluoromethane (PFC-14)	CF_4 (CF_4)	88.0043	7380	75-73-0
2,2,2-trifluoroacetyl fluoride	C_2F_4O (CF_3CFO)	116.01	Low (gas dissolves in water)	354-34-7
2,2,2-trifluoro acetaldehyde	C_2HF_3O (CF_2HCFO)	98.02	~0.2	75-90-1
Trifluoromethyl hypo fluorite	CF_4O (CF_3OF)	104.004	~1	373-91-1

gasses, the same flow rates of C_2F_4O (30–110 sccm)/Ar (150 sccm) and C_2HF_3O(30–110 sccm)/Ar(150 sccm) were introduced into the process chamber. In addition, as an additional alternative gas, CF_4O was also initially investigated with a gas flow rates of CF_4O (30–110 sccm)/Ar (150 sccm). Table 1 shows the GWP 100 $_{yr}$ index for the fluorocarbon gasses in the experiment. CF_4 has a high GWP of 7380, while the other gasses, C_2F_4O, C_2HF_3O, and CF_4O have GWP values close to ~0 [27–31].

The etch depths of SiO_x, SiN_x, and PR were measured using a step profilometer (Tencor, Alpha Step 500). The etch profiles were observed with a field emission scanning electron microscope (FE-SEM; Hitachi, S-4700), which was also used to measure CD loss. The surface roughness of SiO_x and SiN_x before and after etching was measured using an atomic force microscope (AFM; NanoWizard Ultra Speed). The dissociated species generated by the fluorocarbon plasma were analyzed using OES (ANDOR technology, SR-ASZ-0103). Additionally, positive ions in the plasmas were measured using a QMS (Hiden Analytical, PSM 500). The composition and binding state of the etched material surfaces after the etching were observed using XPS (VG Microtech Inc., ESCA2000; X-Ray Gun, Al 180 W [12 kV, 15 mA]). Additionally, root mean square (RMS) surface roughness after etching was measured using AFM and the concentration of gas species in the exhaust line was measured using a FT-IR spectroscope located near the dry pump, and which were used to calculate MMTCE, that is, the total GWP of the exhausted gas, using the following equation. The MMTCEs were calculated using GWP_{100yr}, which represents the GWPs integrated over a 100-year time horizon, and M_i, the total mass of the emitted HFCs and PFCs as measured by FT-IR during the process [32–34].

$$\text{MMTCE}=\sum_i \frac{12}{44}\times\frac{M_i\times GWP_{100yr}}{10^9}$$

3 | Results and Discussion

3.1 | SiO_x, SiN_x, and PR Etching

The blank wafer etch characteristics of SiO_x, SiN_x, and PR were measured using alternative gasses such as C_2F_4O, C_2HF_3O, and CF_4O in addition to CF_4/O_2, and the results are shown in Figure 2. 150 sccm of Ar was added as an additive gas. For CF_4 only, 5 sccm of O_2 was added in addition to Ar/fluorocarbon gas flow. Other process conditions such as ICP power, DC bias voltage, chamber pressure, and substrate temperature were maintained at 2000 W, −500 V, 30 mTorr, and RT, respectively. As shown in Figure 2a–d, as the gas flow rates were increased, the etch rates of SiN_x, SiO_x, and PR were increased for all the gasses such as CF_4/O_2, C_2F_4O, C_2HF_3O, and CF_4O. Compared to CF_4/O_2, C_2F_4O and C_2HF_3O exhibited lower etch rates for SiO_x, SiN_x, and PR across the entire gas flow rate range, while, for CF_4O/Ar, the etch rates of SiO_x, SiN_x, and PR were higher for the entire gas flow rate range investigated compared to the previous three gasses. Therefore, the etch rates were observed in the order of $CF_4O > CF_4/O_2 > C_2F_4O > C_2HF_3O$ across the investigated gas flow rate range. In the case of etch selectivities, as shown in Figure 2e–h, C_2HF_3O exhibited the higher etch selectivities of SiN_x/SiO_x and SiO_x/PR compared to C_2F_4O, while C_2F_4O showed the higher etch selectivities of SiN_x/SiO_x and SiO_x/PR compared to CF_4/O_2. CF_4O exhibited the lowest etch selectivity for both SiN_x/SiO_x and SiO_x/PR among the four gasses. Therefore, in general, the etch selectivity was observed in the order of $C_2HF_3O > C_2F_4O > CF_4/O_2 > CF_4O$ across the studied gas flow rate range. When the gas flow rate was fixed at 70 sccm, the etch rates of SiO_x were approximately ~225, ~197, ~165, and ~329 nm/min with CF_4/O_2, C_2F_4O, C_2HF_3O, and CF_4O, respectively. For the etch selectivities of SiN_x/SiO_x, the values were ~1.9, ~2.0, ~2.0, and ~1.7, while those for the SiO_x/PR were ~0.8, ~1.0, ~1.9, and ~0.3 for CF_4/O_2, C_2F_4O, C_2HF_3O, and CF_4O, respectively. Therefore, among the three alternative gases, C_2F_4O showed the most similar etch rates and etch selectivities compared to CF_4/O_2 for the investigated gas range while C_2HF_3O shows a little lower etch rate and a slightly higher etch selectivity compared to CF_4/O_2.

Using the 1335 nm thick dielectric layers consisted of $SiN_x/SiO_x/SiN_x/SiO_x$ deposited on amorphous silicon/glass substrates and patterned with ~1.8 um thick PR, contact holes were etched using CF_4/O_2, C_2F_4O, C_2HF_3O, and CF_4O, and the cross-sectional SEM images of the etched SiN_x/SiO_x contact features are shown in Figure 3a–d with PR and, in Figure 3e–g, after PR strip, respectively. Not to damage the amorphous silicon surface at the bottom of the etch hole, the etching was stopped before the exposure of amorphous silicon by leaving a ~15 nm thick SiO_x on amorphous silicon. To etch 1320 nm deep $SiN_x/SiO_x/SiN_x/SiO_x$, CF_4/O_2 required 4 min while C_2F_4O and C_2HF_3O required ~5 and ~6.3 min, respectively. In the case of CF_4O, ~353 nm deep SiN_x/SiO_x etching could be obtained for ~1.16 min but, due to the low etch selectivity over PR, etching was stopped after the etching ~353 nm.

16128869, 2025, 10, Downloaded from https://onlinelibrary.wiley.com/doi/10.1002/ppap.70068 by Sungkyunkwan University, Wiley Online Library on [03/02/2026]. See the Terms and Conditions (https://onlinelibrary.wiley.com/terms-and-conditions) on Wiley Online Library for rules of use; OA articles are governed by the applicable Creative Commons License

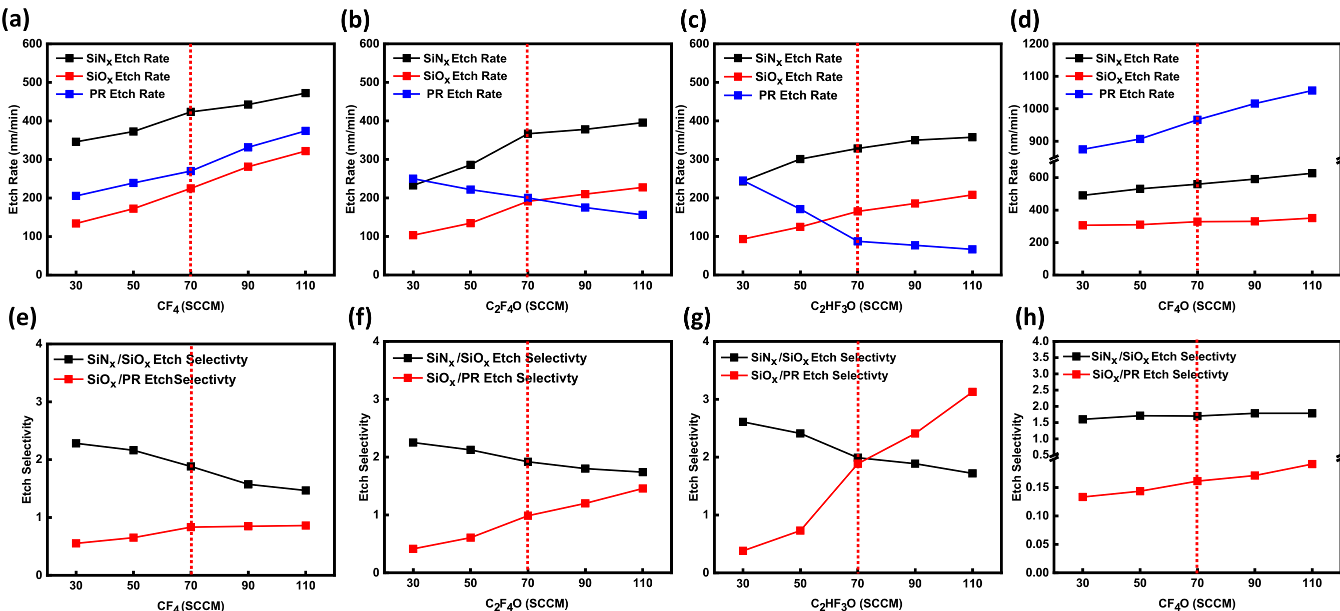

FIGURE 2 | Etch rates of SiO_x, SiN_x, and PR for (a) CF_4/O_2, (b) C_2F_4O, (c) C_2HF_3O, and (d) CF_4O. Etch selectivities of SiN_x/SiO_x and SiO_x/PR for (e) CF_4/O_2, (f) C_2F_4O, (g) C_2HF_3O, and (h) CF_4O. For CF_4/O_2, the O_2 flow rate was fixed at 5 sccm. For all gases, 150 sccm Ar was added, and other process conditions such as ICP power, DC bias voltage, and chamber pressure were maintained at 2000 W, −500 V, and 30 mTorr.

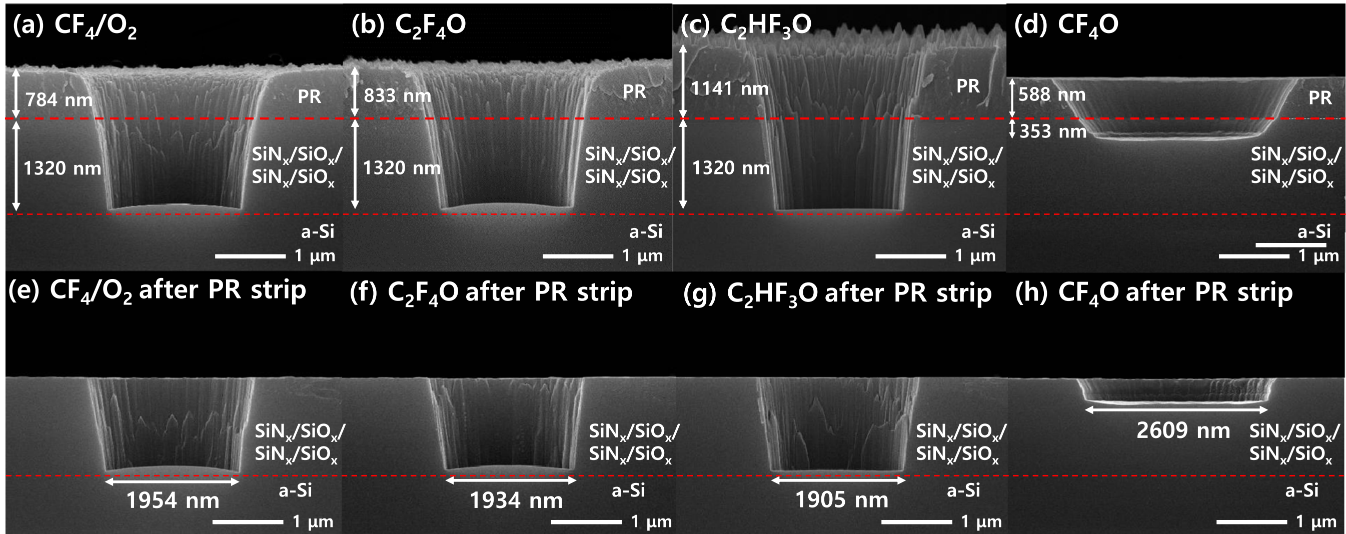

FIGURE 3 | Cross-sectional SEM images of PR masked SiN_x/SiO_x contact holes etched using (a) CF_4 (70 sccm)/O_2 (5 sccm), (b) C_2F_4O (70 sccm), (c) C_2HF_3O (70 sccm), and (d) CF_4O (70 sccm). 150 sccm of Ar was added for all conditions. (e) CF_4/O_2, (f) C_2F_4O, (g) C_2HF_3O, and (h) CF_4O are the SEM images after PR mask strip.

As shown in Figure 3a,b,e,f, the $SiN_x/SiO_x/SiN_x/SiO_x$ etch profiles of CF_4/O_2 and C_2F_4O were similar, even though the $SiN_x/SiO_x/SiN_x/SiO_x$ etch rate using C_2F_4O was slightly lower. Due to the slightly higher etch selectivity over PR for C_2F_4O compared to CF_4/O_2, thicker PR (~833 nm) remained on the etched $SiN_x/SiO_x/SiN_x/SiO_x$ contact hole and smaller bottom hole sizes (~1934 nm) could be observed compared to CF_4/O_2(784 nm PR and ~1954 nm bottom hole size). However, micro-trenching was observed at the bottom of contact holes for both CF_4/O_2 and C_2F_4O, possibly due to the high ion flux during the etching at the edge of the hole by ions reflected from the sloped sidewall. In the case of C_2HF_3O, as shown in Figure 3c,g, ~1141 nm thick PR remained after etching due to the higher etch selectivity over PR of ~2.21 compared to CF_4/O_2. In addition, a more anisotropic $SiN_x/SiO_x/SiN_x/SiO_x$ contact etch profile with the smallest contact bottom hole size of ~1905 nm and no micro-trenching at the bottom of the contact hole could be observed due to the highest etch selectivity over PR with C_2HF_3O. However, at the top of the PR, roughening of the PR surface could be observed, possibly due to the damage of the PR with H radicals dissociated from C_2HF_3O. Figure 3d shows the $SiN_x/SiO_x/SiN_x/SiO_x$ contact hole etched ~353 nm using CF_4O for ~1.16 min, while Figure 3h presents the corresponding SEM image after PR stripping. Due to the low etch selectivity over PR with CF_4O, $SiN_x/SiO_x/SiN_x/SiO_x$ etching was stopped after etching ~353 nm and, at this condition, only ~588 nm thick PR

16128869, 2025, 10, Downloaded from https://onlinelibrary.wiley.com/doi/10.1002/ppap.70068 by Sungkyunkwan University, Wiley Online Library on [03/02/2026]. See the Terms and Conditions (https://onlinelibrary.wiley.com/terms-and-conditions) on Wiley Online Library for rules of use; OA articles are governed by the applicable Creative Commons License

was remaining. The $SiN_x/SiO_x/SiN_x/SiO_x$ etch profile was severely slopped and the etched bottom was significantly expanded to ~2609 nm. It was found that CF_4O was not effective in the etching of PR masked $SiN_x/SiO_x/SiN_x/SiO_x$ contact hole; therefore, further investigation was conducted only with CF_4/O_2, C_2F_4O, and C_2HF_3O.

3.2 | Plasma Analysis

For understanding the above etch characteristics, plasma analysis was performed. Figure 4a shows the OES data of the plasmas generated with the reactive gases of CF_4/O_2, C_2F_4O, and C_2HF_3O normalized to Ar. The process conditions were set with an ICP source power of 2000 W, a DC bias voltage of −500 V, and a process pressure of 30 mTorr. As reactive gases, CF_4 (70 sccm)/O_2 (5 sccm), C_2F_4O (70 sccm), and C_2HF_3O (70 sccm) were used with the Ar flow rate of 150 sccm. As shown in Figure 4a, radical peaks such as F, CF_2, and CH could be identified at 703.7, 251.9, and 388 nm, respectively, from the OES data [26, 35]. The intensity ratios of F/Ar, CF_2/Ar, and CH/Ar for the reactive gases from Figure 4a are shown in Figure 4b. As shown in Figure 4b, the intensity of F/Ar was similar for all three gases, but the ratios of CF_2/Ar increased in the order of CF_4/O_2, C_2F_4O, and C_2HF_3O. Figure 4c shows the CF_2/F ratio of intensity, which is related to the ratio of polymerizing species/etching species, and as shown in Figure 4c, the ratio of CF_2/F was also slightly increased in the order of CF_4/O_2, C_2F_4O, and C_2HF_3O. For CH radicals observed for C_2HF_3O plasma can also participate in polymerizing the surfaces. The increase in CF_2/F and (CF_2 + CH)/F ratios implies a higher polymerizing to etching species ratio, consistent with the increased surface polymer formation and reduced etch rates observed for C_2HF_3O. Therefore, the lower SiN_x/SiO_x etch rates, and the higher etch selectivities of SiO_x over PR in the order of $CF_4/O_2 < C_2F_4O < C_2HF_3O$ observed in Figure 2e,f and Figure 3a,c, respectively, are believed to be related to the higher polymerizing species compared to the etching species generated in the plasma.

In addition to radical analysis by OES, the positive reactive ions in the plasmas were analyzed using QMS for the process conditions in Figure 4. Figure 5a shows the mass spectra of positive ions detected for the plasmas generated with CF_4/O_2, C_2F_4O, and C_2HF_3O using QMS. Various positive ions dissociated from CF_4/O_2, C_2F_4O, and C_2HF_3O including species such as CF^+, CHF^+, and CF_3^+ which could not be measured by OES could be observed; however, F^+ was not detected due to its low possibility in positive ion formation in the plasma. H^+ and CHF^+ ions were detected only in C_2HF_3O. Figure 5b presents the intensities of CF^+, CHF^+, CF_2^+, and CF_3^+ ions from (a) for CF_4/O_2, C_2F_4O, and C_2HF_3O. Similar to the OES results in

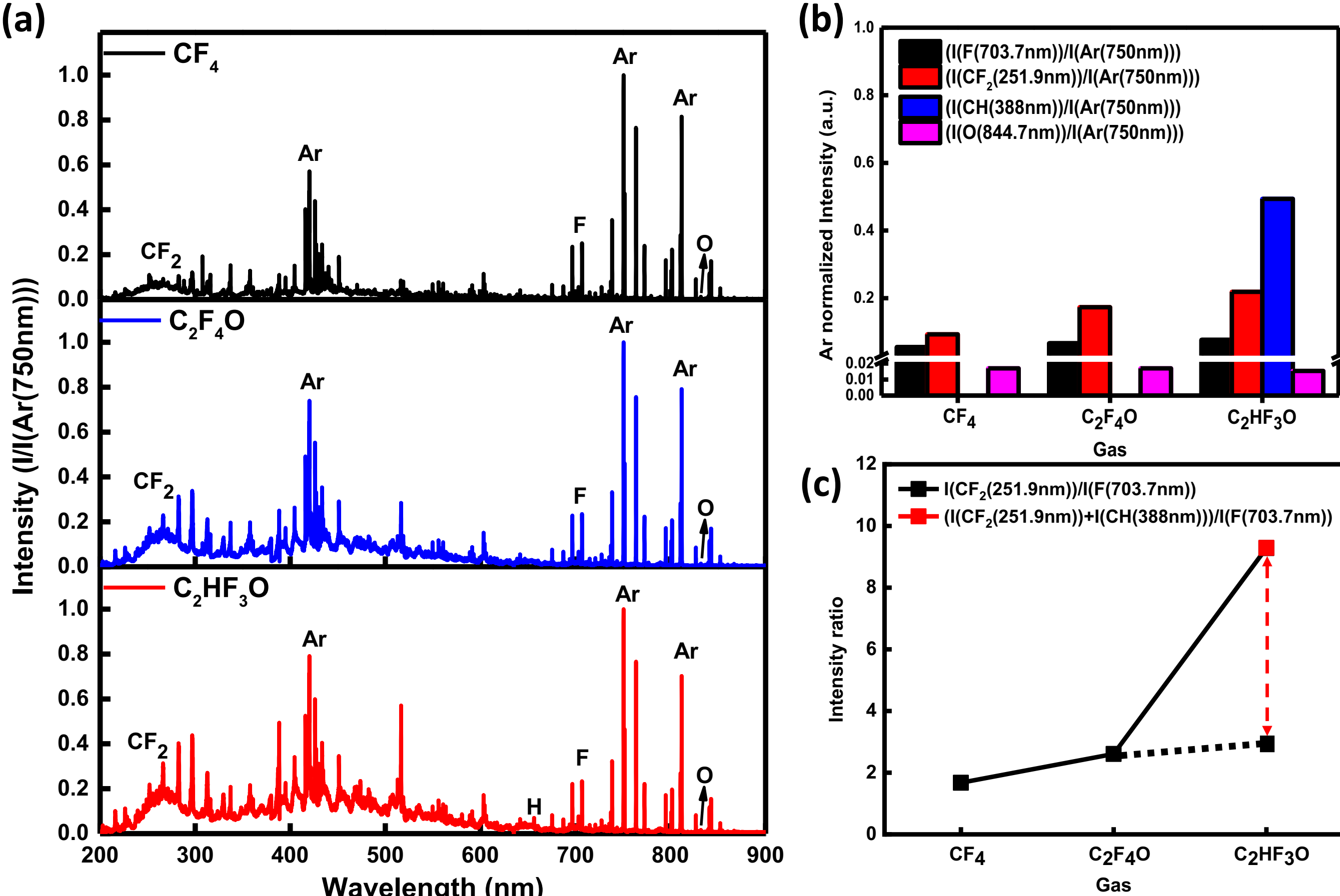

FIGURE 4 | (a) OES of the plasmas generated with CF_4/O_2, C_2F_4O, and C_2HF_3O normalized to Ar. (b) Radical intensities of F, CF_2, and CH measured after normalization to Ar, and (c) intensity ratios of CF_2/F and (CF_2 + CH)/F. ICP source power of 2000 W, a DC bias of −500 V, 30 mTorr, and Ar flow rate of 150 sccm, and for reactive gases, CF_4 (70 sccm)/O_2 (5 sccm), C_2F_4O (70 sccm), and C_2HF_3O (70 sccm) were used.

16128869, 2025, 10, Downloaded from https://onlinelibrary.wiley.com/doi/10.1002/ppap.70068 by Sungkyunkwan University, Wiley Online Library on [03/02/2026]. See the Terms and Conditions (https://onlinelibrary.wiley.com/terms-and-conditions) on Wiley Online Library for rules of use; OA articles are governed by the applicable Creative Commons License

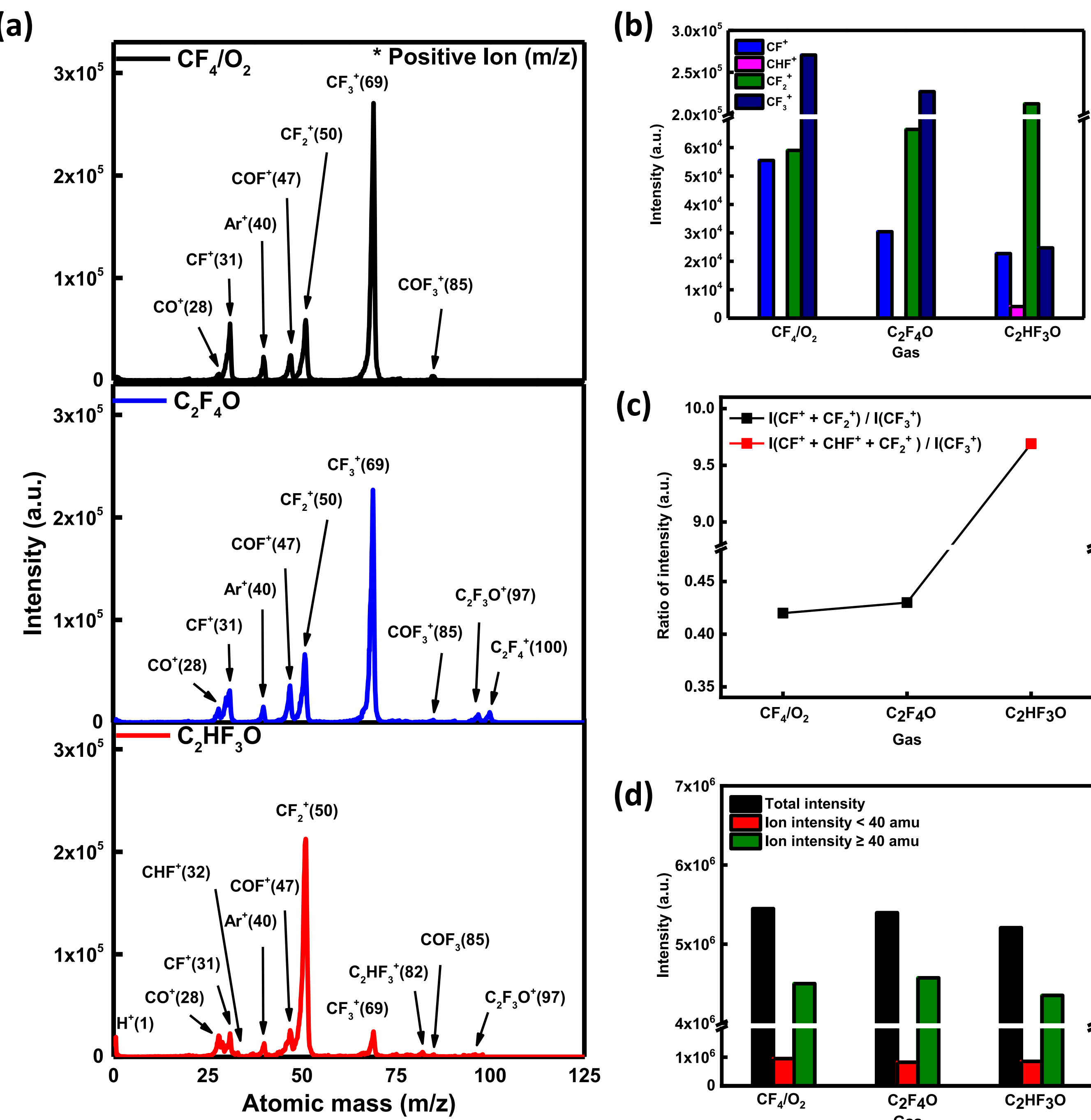

FIGURE 5 | (a) Positive ion data measured by QMS for CF_4/O2, C_2F_4O, and C_2HF_3O. (b) Positive ion intensity of CF^+, CHF^+, $CF_2{}^+$, and $CF_3{}^+$ for CF_4/O_2, C_2F_4O, and C_2HF_3O extracted from (a). (c) Positive ion intensity ratios of $(CF^+ + CHF^+ + CF_2{}^+)/CF_3{}^+$ and $(CF^+ + CF_2{}^+)/CF_3{}^+$ from (b). (d) Sum of positive ion mass intensities with mass below 40 amu and mass above 40 amu, along with the sum of total positive ion mass intensities.

Figure 4b, the intensity of $CF_2{}^+$ increased in the order of $CF_4/O_2 < C_2F_4O < C_2HF_3O$. However, CF^+ intensity slightly decreased in the order of $CF_4/O_2 > C_2F_4O > C_2HF_3O$, while $CF_3{}^+$ intensity decreased significantly, especially for C_2HF_3O. When the ratio of $(CF^+ + CHF^+ + CF_2{}^+)/CF_3{}^+$, which is partially related to polymerizing ion species/etching species was measured, as shown in Figure 5c, the ratios were increased in the order of $CF_4/O_2 < C_2F_4O < C_2HF_3O$ similar to the result of Figure 4c indicating more polymerizing ion species in addition to polymerizing radical species from the plasma. More polymerizing ion species in addition to polymerizing radical species from plasma are believed to be related to the lower SiN_x/SiO_x etch rates, and the higher etch selectivities of SiN_x/SiO_x over PR observed in Figure 2e,f and Figure 3a,c in the order of $CF_4/O2 < C_2F_4O < C_2HF_3O$.

To understand the ion bombardment effect on the $SiN_x/SiO_x/SiN_x/SiO_x$ contact hole etch profiles, the number of heavy ions having mass higher than 40 amu and the number of light ions having mass lower than 40 amu were compared in addition to

16128869, 2025, 10, Downloaded from https://onlinelibrary.wiley.com/doi/10.1002/ppap.70068 by Sungkyunkwan University, Wiley Online Library on [03/02/2026]. See the Terms and Conditions (https://onlinelibrary.wiley.com/terms-and-conditions) on Wiley Online Library for rules of use; OA articles are governed by the applicable Creative Commons License

the total number of positive ions, and the results are shown in Figure 5d [36]. As shown in Figure 5d, the sum of positive ions with mass below 40 amu showed no significant differences for all three gasses, but for the sum of positive ions with mass above 40 amu, CF_4/O_2 and C_2F_4O were similar, whereas C_2HF_3O had a lower intensity. Therefore, the total number of positive ions was similar for CF_4/O_2 and C_2F_4O, but lower for C_2HF_3O. The higher ion bombardment effect with a higher number of heavy mass ions observed for CF_4/O_2 and C_2F_4O, in addition to the greater ion flux to the contact bottom edge due to the reflection of ions at the sloped sidewall appears to be related to the formation of micro-trenching. On the contrary, for C_2HF_3O, no such micro-trenching was observed at the contact bottom edge possibly due to no such high bombardment effect, in addition to the no higher ion flux to the contact bottom edge by the reflection of ions at the anisotropic sidewall.

3.3 | Surface Analysis

The surface composition after etching with CF_4/O_2, C_2F_4O, and C_2HF_3O was measured by XPS, and the results are shown in Figure 6 for the surfaces of (a) SiO_x, (b) SiN_x, and (c) PR. The etch conditions are the same as those in Figure 4. As shown in Figure 6, the carbon percentage on the surfaces of SiO_x, SiN_x, and PR was increased while decreasing silicon percentage on the etched surfaces of SiO_x and SiNx in the order of $CF_4/O_2 < C_2F_4O < C_2HF_3O$, which indicates a thicker carbon-rich polymer layer on the material's surface in the order of $CF_4/O_2 < C_2F_4O < C_2HF_3O$. The F percentage was the lowest for C_2HF_3O, possibly due to the removal of F on the materials' surfaces by forming HF with H from C_2HF_3O.

The XPS carbon peak was further analyzed to understand the characteristics of the polymer deposited on the material's surface. Figure 7 shows the XPS C1s narrow-scan data for SiN_x, SiO_x, and PR after etching with (a–c) CF_4/O_2, (d–f) C_2F_4O, and (g–i) C_2HF_3O. On all surfaces, carbon bonding peaks such as C–C (~285 eV), C–CF (~287.5 eV), C–F (~289.5 eV), and C–CF_2 (~291.8 eV) could be observed [37]. As shown in Figure 7, more C–C and C–CF bonds compared to C–F and C–F_2 bonds were observed in the order of $SiO_x < SiN_x <$ PR for the same gas and also in the order of $CF_4/O_2 < C_2F_4O < C_2HF_3O$ for the same material surface, indicating the formation of carbon-rich polymer on the material surface due to more carbon in the molecular structure of C_2F_4O compared to CF_4/O_2 and additional CH-bonds for C_2HF_3O. The rise in C-C and C–CF bonding intensities for C_2HF_3O indicates the formation of a

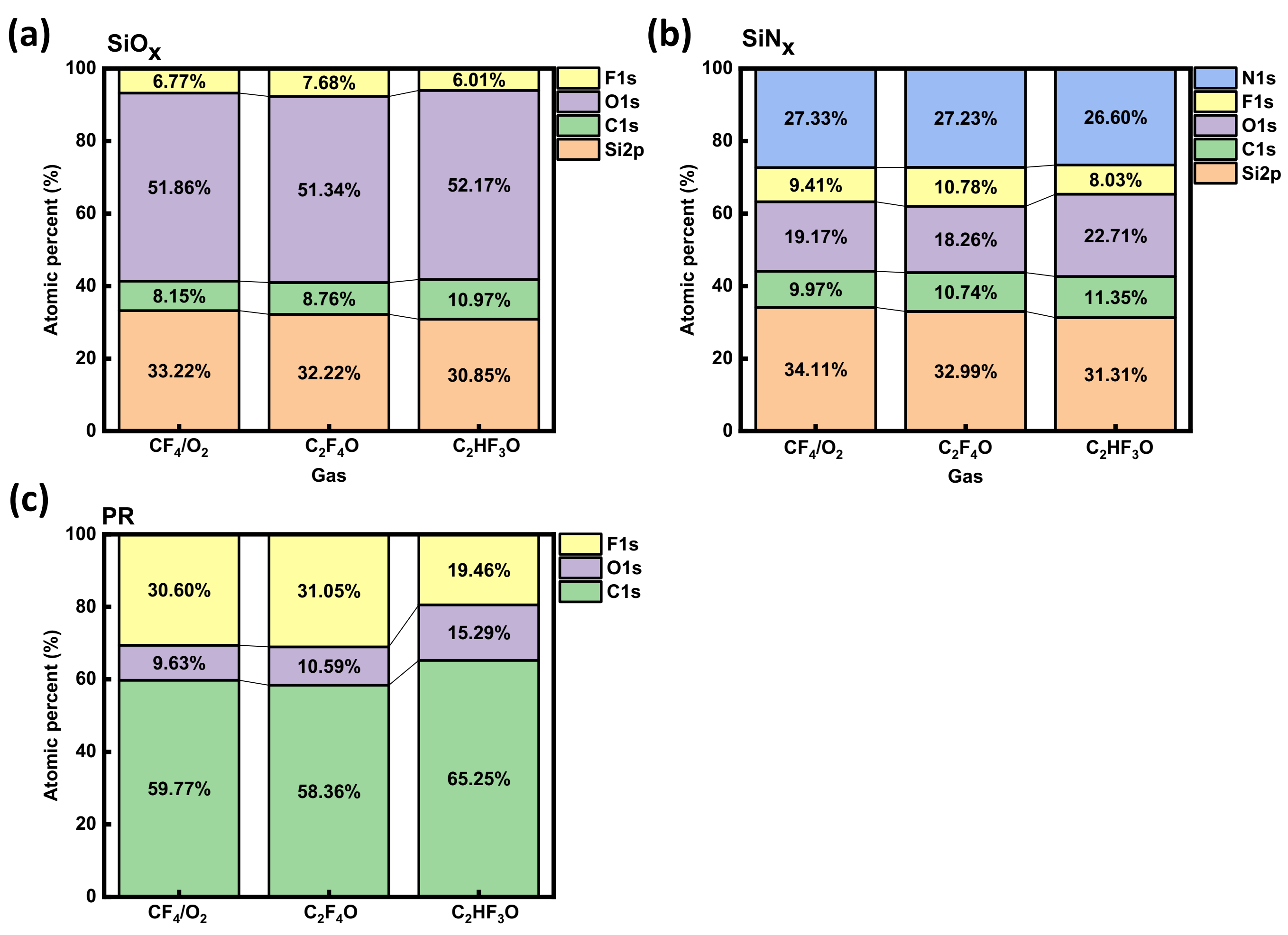

FIGURE 6 | Surface composition measured by XPS after etching of (a) SiO_x, (b) SiN_x, and (c) PR with CF_4/O_2, C_2F_4O, and C_2HF_3O. The etch conditions are the same as those in Figure 4.

16128869, 2025, 10, Downloaded from https://onlinelibrary.wiley.com/doi/10.1002/ppap.70068 by Sungkyunkwan University, Wiley Online Library on [03/02/2026]. See the Terms and Conditions (https://onlinelibrary.wiley.com/terms-and-conditions) on Wiley Online Library for rules of use; OA articles are governed by the applicable Creative Commons License

FIGURE 7 | XPS C1s narrow-scan data for the surfaces of SiN_x, SiO_x, and PR etched with CF_4/O2, C_2F_4O, and C_2HF_3O in Figure 6. (a–c) CF_4/O_2, (d–f) C_2F_4O, and (g–i) C_2HF_3O gasses.

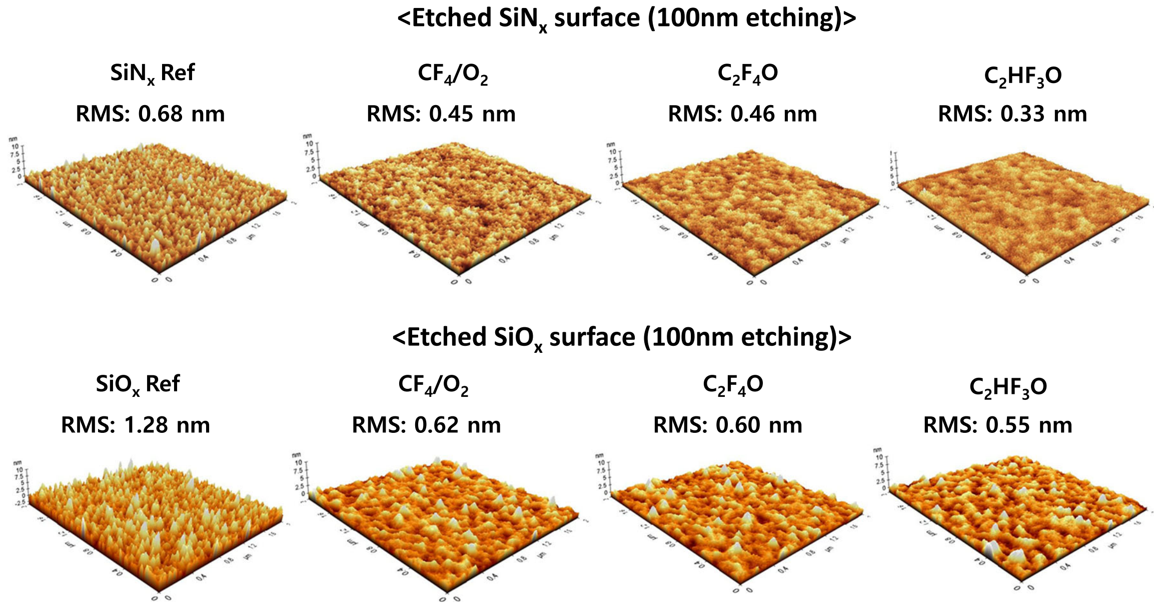

FIGURE 8 | RMS surface roughness measured by AFM after etching 100 nm thick SiN_x and SiO_x using CF_4/O_2, C_2F_4O, and C_2HF_3O. The process conditions are the same as those in Figure 4.

16128869, 2025, 10, Downloaded from https://onlinelibrary.wiley.com/doi/10.1002/ppap.70068 by Sungkyunkwan University, Wiley Online Library on [03/02/2026]. See the Terms and Conditions (https://onlinelibrary.wiley.com/terms-and-conditions) on Wiley Online Library for rules of use; OA articles are governed by the applicable Creative Commons License

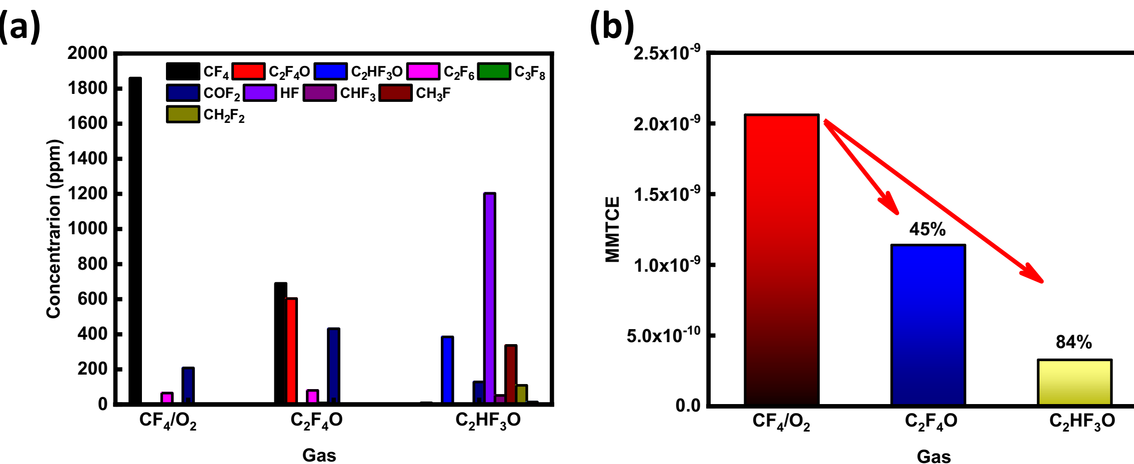

FIGURE 9 | (a) Concentration of various recombined fluorocarbon gases measured using FTIR at pumping line during the etching using CF_4/O_2, C_2F_4O, and C_2HF_3O. (b) MMTCE calculated with (a) during the etching with CF_4/O_2, C_2F_4O, and C_2HF_3O. The process conditions were the same as those in Figure 4.

denser polymer film, which acts as a passivation layer enhancing selectivity over PR.

The RMS surface roughness after the etching of ~100 nm thick SiO_x and SiN_x using CF_4/O_2, C_2F_4O, and C_2HF_3O were measured by AFM and the results are shown in Figure 8. The RMS surface roughness values before the etching were ~0.68 nm for SiN_x and ~1.28 nm for SiO_x. After the etching of ~100 nm, the surface roughness values were improved for all the gasses by showing 0.45, 0.4, 0.33 nm on the etched SiN_x, and by showing 0.62, 0.60, and 0.55 nm on the etched SiO_x with CF_4/O_2, C_2F_4O, and C_2HF_3O, respectively. Therefore, the polymer layer formed during the etching did not cause any micromasking during the etching, and smoother etched surfaces could be obtained for a flat contact bottom.

3.4 | MMTCE

Figure 9a shows the concentrations of various fluorocarbon gasses measured at the pumping line near the dry pump using FT-IR, which were formed by the recombination of the dissociated fluorocarbon etch gasses, including the etch gas itself during the etching using CF_4/O_2, C_2F_4O, and C_2HF_3O. The process conditions were the same as those in Figure 4. As shown in Figure 9a, in the exhaust line, during the etching with CF_4/O_2, C_2F_6 ($GWP100_{yr} = 12400$) and COF_2 ($GWP100_{yr} = 1$) were observed in addition to CF_4 itself. In the case of etching with C_2F_4O, in addition to C_2F_4O, recombined CF_4, C_2F_6, and COF_2, which were the same species as with CF_4/O_2, were observed. For, C_2HF_3O, in addition to undissociated C_2HF_3O, COF_2, HF($GWP100_{yr} = 0$), CHF_3($GWP100_{yr} = 14600$), CH_3F ($GWP100_{yr} = 135$), and CH_2F_2($GWP100_{yr} = 771$) were observed [38–41]. The significantly higher HF signal in the exhaust for C_2HF_3O suggests efficient scavenging of fluorine by hydrogen, which indirectly leads to suppressed etching and enhanced carbon retention on the surface. Using the concentration information in Figure 9a, the MMTCE, which is the total GWPs, was calculated using the equation shown in the experimental section, and the results are shown in Figure 9b. As shown in Figure 9b, when the MMTCEs were calculated, C_2F_4O showed a reduction of ~45% and C_2HF_3O showed a reduction of ~84% in MMTCE compared to CF_4/O_2. Therefore, these alternative gasses showed lower total GWPs compared to CF_4/O_2 and released fewer high-GWP gasses to the exhaust line, making them environmentally friendly, while showing similar etch characteristics for C_2F_4O and better etch profiles and etch selectivity over PR for C_2HF_3O.

4 | Conclusions

The etching characteristics using fluorocarbon gasses with low GWPs were investigated as alternatives to CF_4, which was traditionally used for the etching of dielectric materials such as SiO_x and SiN_x in display device processing. By employing C_2F_4O and C_2HF_3O chemistries instead of CF_4/O_2, similar etch characteristics such as etch rates, etch selectivity over PR, and etch profiles for C_2F_4O and, better etch characteristics such as etch profiles and etch selectivity over PR for C_2HF_3O could be achieved. Plasma characterization revealed that polymerizing species in the plasma such as CF_2, CH, CF^+, CHF^+, and CF_2^+ were higher than etching species such as F and CF_3^+, and the surface characterization also showed higher C−C and C−CF bonds compared to CF and CF_2 bonds on the etched material surface, which indicated more carbon-rich polymer layer on the etched material surface in the order of $CF_4/O_2 < C_2F_4O < C_2HF_3O$. Therefore, more selective etching was observed in the order of $CF_4/O_2 < C_2F_4O < C_2HF_3O$, and the etch characteristics of C_2F_4O were more similar to CF_4/O_2 compared to C_2HF_3O. When the MMTCE, which is the total GWPs, was measured during the etching with CF_4/O_2, C_2F_4O, C_2HF_3O, the etching with C_2F_4O showed a reduction of ~45% and C_2HF_3O a reduction of approximately ~84% in MMTCE compared to CF_4/O_2. Therefore, it is believed that the dielectric etching with CF_4/O_2 can be replaceable with C_2F_4O or C_2HF_3O for applications in next-generation display and semiconductor manufacturing while decreasing the GWPs.

Author Contributions

Jun Won Jeong: conceptualization, investigation, methodology, formal analysis. **Jong Woo Hong:** conceptualization, investigation, methodology, formal analysis, validation, writing – original draft.

16128869, 2025, 10, Downloaded from https://onlinelibrary.wiley.com/doi/10.1002/ppap.70068 by Sungkyunkwan University, Wiley Online Library on [03/02/2026]. See the Terms and Conditions (https://onlinelibrary.wiley.com/terms-and-conditions) on Wiley Online Library for rules of use; OA articles are governed by the applicable Creative Commons License

Hyeong Joon Eoh: writing – review and editing. **Chan Ho Kim:** writing – review and editing. **Kyung Lim Kim:** investigation, resources. **Sung Hyun Kim:** conceptualization, data curation, project administration, supervision, methodology investigation, and resources. **Young Woo Jeon:** project administration. **Jong Soon Park:** conceptualization, data curation. **Hyun Min Cho:** investigation, resources. **Yu Gwang Jeong:** conceptualization, data curation, project administration, supervision, methodology. **Da Woon Jung:** conceptualization, data curation, project administration, supervision, methodology. **Yun Jong Yeo:** investigation. **Geun Young Yeom:** conceptualization, data curation, project administration, supervision, writing – review and editing. **Dong Woo Kim:** conceptualization, data curation, project administration, supervision, writing – review and editing.

Acknowledgments

This work was supported by Samsung Display Co. Ltd. (S-2024-1085-000-01) and the Technology Innovation Program Development Program-Development of core technology in Carbon Neutrality (RS-2023-00265858, Development of alternative PFC gas with low GWP value under 150 for OLED display oxide TFT insulator patterning) funded by the Ministry of Trade, Industry & Energy (MOTIE, Korea).

Conflicts of Interest

The authors declare no conflicts of interest.

Data Availability Statement

Data will be made available on request.

References

1. S. Li, R. Yao, and H. Ning, "LTPS-TFT Process for OLED and Some Issues Generated From the Manufacturing." *Digest of Technical Papers* (John Wiley and Sons Inc, 2018), 625–631, https://doi.org/10.1002/SDTP.12801.

2. T. Kugimiya, Y. Yoneda, E. Kusumoto, H. Gotoh, M. Ochi, and N. Kawakami, "24.2: Single Layer Al-Ni-La-Si Interconnections for Source and Drain of LTPS-TFT LCDs Using Direct Contacts With Both ITO and Poly-Si," *SID Symposium Digest of Technical Papers* 39 (2008): 329–332, https://doi.org/10.1889/1.3069660.

3. J. H. Ye, C. L. Huang, M. Y. Chen, et al., "Development of Crystalline IGZO and LTPS Hybrid TFTs Array Technology." *Digest of Technical Papers* (Blackwell Publishing Ltd, 2017), 600–603, https://doi.org/10.1002/sdtp.11710.

4. H. U. Huzaibi, X. Shi, D. Geng, N. Lu, L. Li, and M. Liu, "Charge Transport Mechanism in Low Temperature Polycrystalline Silicon (LTPS) Thin-Film Transistors," *AIP Advances* 9 (2019): 025321, https://doi.org/10.1063/1.5082994.

5. S. I. Hsieh, H. T. Chen, Y. C. Chen, C. L. Chen, J. X. Lin, and Y. C. King, "Reliability and Memory Characteristics of Sequential Laterally Solidified Low Temperature Polycrystalline Silicon Thin Film Transistors With an Oxide-Nitride-Oxide Stack Gate Dielectric," *Japanese Journal of Applied Physics* 45 (2006): 3154–3158, https://doi.org/10.1143/JJAP.45.3154.

6. L. W. MacDonald, A. C. Lowe, G. Crawford, et al., "Flat Panel Display Manufacturing Wiley-SID Series in Display Technology Display Systems: Design and Applications Digital Image Display: Algorithms and Implementation Gheorghe Berbecel Flexible Flat Panel Displays Introduction to Flat Panel Displays," https://onlinelibrary.wiley.com/doi/.

7. T. Kaneko, T. Nakamura, and H. Kimura, "(Invited) Present and Future of LTPS Technology," *ECS Transactions* 75 (2016): 3–12, https://doi.org/10.1149/07510.0003ecst.

8. "AR6 WGI Report-List of Corrigenda to be Implemented," (2023), https://github.com/IPCC-WG1/Chapter-7.

9. B. Kim, D. W. Lee, and K. H. Kwon, "Prediction of Etch Microtrenching Using a Neural Network," *Journal of Applied Physics* 96 (2004): 3612–3616, https://doi.org/10.1063/1.1789276.

10. A. P. Mahorowala and H. H. Sawin, "Etching of Polysilicon in Inductively Coupled Cl2 and HBr Discharges. III. Photoresist Mask Faceting, Sidewall Deposition, and Microtrenching," *Journal of Vacuum Science & Technology B: Microelectronics and Nanometer Structures Processing, Measurement, and Phenomena* 20 (2002): 1077–1083, https://doi.org/10.1116/1.1481868.

11. J. W. Hong, Y. H. Kim, H. J. Kim, et al., "Etched Characteristics of Nanoscale TiO_2 Using C_4F_8-Based and BCl_3-Based Gases," *Materials Science in Semiconductor Processing* 164 (2023): 107617, https://doi.org/10.1016/j.mssp.2023.107617.

12. Y. Kim, S. Kim, H. Kang, S. You, C. Kim, and H. Chae, "Low Global Warming $C_4H_3F_7O$ Isomers for Plasma Etching of SiO_2 and Si_3N_4 Films," *ACS Sustainable Chemistry & Engineering* 10 (2022): 10537–10546, https://doi.org/10.1021/acssuschemeng.2c01705.

13. ALICE Collaboration, "Joint Statement of the 25th Meeting of the World Semiconductor Council (WSC)," *Nature* 606 (2022): 287–292.

14. H. W. Tak, H. J. Lee, L. Wen, et al., "Effect of Hydrofluorocarbon Structure of $C_3H_2F_6$ Isomers on High Aspect Ratio Etching of Silicon Oxide," *Applied Surface Science* 600 (2022): 154050, https://doi.org/10.1016/j.apsusc.2022.154050.

15. J. Woo Hong, H. Woo Tak, N. Il Cho, et al., "Reactive Ion Etching of Indium Gallium Zinc Oxide (IGZO) and Chamber Cleaning Using Low Global Warming Potential Gas," *Applied Surface Science* 671 (2024): 160692, https://doi.org/10.1016/j.apsusc.2024.160692.

16. J. W. Hong, H. M. Cho, Y. G. Jeong, et al., "Indium Tin Oxide Etch Characteristics Using C_xH_{2x+2}(x=1,2,3)/Ar," *Materials Science in Semiconductor Processing* 160 (2023): 107395, https://doi.org/10.1016/j.mssp.2023.107395.

17. J. Kim, H. Kang, Y. Kim, M. Jeon, and H. Chae, "Low Global Warming $C_5F_{10}O$ Isomers for Plasma Atomic Layer Etching and Reactive Ion Etching of SiO_2 and Si_3N_4," *Plasma Processes and Polymers* 21 (2024): 2300216, https://doi.org/10.1002/ppap.202300216.

18. S. You, E. Sun, H. Chae, and C. K. Kim, "Effect of Discharge Gas Composition on SiC Etching in an HFE-347mmy/O2/Ar Plasma," *Materials* 17 (2024): 3917, https://doi.org/10.3390/ma17163917.

19. H. K. Lee, K. S. Chung, and J. S. Yu, "Selective Etching of Thick Si_3N_4, SiO_2 and Si by Using CF_4/O_2 and C_2F_6 Gases With or Without O_2 or Ar Addition," 2009.

20. S. C. Jeon, D. Y. Kong, D. S. Pyo, et al., "A Study on Etching of Si_3N_4 Thin Film and the Exhausted Gas Using C_3F_6 Gas for LCD Process," *Journal of the Korean Vacuum Society* 21 (2012): 199–204, https://doi.org/10.5757/jkvs.2012.21.4.199.

21. G. S. Lugani, R. Skaggs, B. Morris, et al., "Direct Emissions Reduction in Plasma Dry Etching Using Alternate Chemistries: Opportunities, Challenges and Need for Collaboration," *IEEE Transactions on Semiconductor Manufacturing* 37 (2024): 445–452, https://doi.org/10.1109/TSM.2024.3444465.

22. S.-N. Hsiao, N. Britun, T.-T.-N. Nguyen, et al., "A Comparative Study on the CF_4/H_2 and HF/H_2 Plasmas for Etching of Highly Hydrogenated SiN Films."

23. T. N. Tran, T. Hayashi, H. Iwayama, M. Sekine, M. Hori, and K. Ishikawa, "Hydrofluoroethane Plasma Etching of SiN, SiO2, and Poly-Si Films With CHF_2CF_3, CF_3CH_3, and CHF_2CH_3," *Applied Surface Science* 684 (2025): 161815, https://doi.org/10.1016/j.apsusc.2024.161815.

24. H. S. Gil, D. S. Kim, Y. J. Jang, et al., "Selective Isotropic Etching of SiO_2 Over Si_3N_4 Using NF_3/H_2 Remote Plasma and Methanol Vapor," *Scientific Reports* 13 (2023): 11599, https://doi.org/10.1038/s41598-023-38359-4.

16128869, 2025, 10, Downloaded from https://onlinelibrary.wiley.com/doi/10.1002/ppap.70068 by Sungkyunkwan University, Wiley Online Library on [03/02/2026]. See the Terms and Conditions (https://onlinelibrary.wiley.com/terms-and-conditions) on Wiley Online Library for rules of use; OA articles are governed by the applicable Creative Commons License

25. J. Woo Hong, H. Woo Tak, N. Il Cho, et al., "Reactive Ion Etching of Indium Gallium Zinc Oxide (IGZO) and Chamber Cleaning Using Low Global Warming Potential Gas," *Applied Surface Science* 671 (2024): 160692, https://doi.org/10.1016/j.apsusc.2024.160692.

26. J. W. Hong, H. M. Cho, Y. G. Jeong, et al., "Indium Tin Oxide Etch Characteristics Using C_xH_{2x+2}(x=1,2,3)/Ar," *Materials Science in Semiconductor Processing* 160 (2023): 107395, https://doi.org/10.1016/j.mssp.2023.107395.

27. W. T. Tsai, "An Overview of Environmental Hazards and Exposure Risk of Hydrofluorocarbons (HFCs)," *Chemosphere* 61 (2005): 1539–1547, https://doi.org/10.1016/j.chemosphere.2005.03.084.

28. R. Lohmann, I. T. Cousins, J. C. Dewitt, et al., "Are Fluoropolymers Really of Low Concern for Human and Environmental Health and Separate From Other PFAS?," *Environmental Science & Technology* 54 (2020): 12820–12828, https://doi.org/10.1021/acs.est.0c03244.

29. K. R. Solomon, G. J. M. Velders, S. R. Wilson, et al., "Sources, Fates, Toxicity, and Risks of Trifluoroacetic Acid and Its Salts: Relevance to Substances Regulated Under the Montreal and Kyoto Protocols," *Journal of Toxicology and Environmental Health, Part B* 19 (2016): 289–304, https://doi.org/10.1080/10937404.2016.1175981.

30. S. Joudan, A. O. De Silva, and C. J. Young, "Insufficient Evidence for the Existence of Natural Trifluoroacetic Acid," *Environmental Science: Processes & Impacts* 23 (2021): 1641–1649, https://doi.org/10.1039/d1em00306b.

31. Y. Saito, H. Yamazaki, and I. Mouri, "Remote-Plasma-Enhanced Reaction Between a Silicon Surface and Trifluoro-Acetyl-Fluoride Gas," *Journal of Vacuum Science & Technology, A: Vacuum, Surfaces, and Films* 19 (2001): 38–40, https://doi.org/10.1116/1.1326942.

32. U. Epa and C. Change Division, "Inventory of US Greenhouse Gas Emissions and Sinks: 1990-2020: Main Text," 1990, https://www.epa.gov/ghgemissions/draft-inventory-us-greenhouse-gas-emissions-.

33. Y. Kim, S. Kim, H. Kang, S. You, C. Kim, and H. Chae, "Low Global Warming $C_4H_3F_7O$ Isomers for Plasma Etching of SiO_2 and Si_3N_4 Films," *ACS Sustainable Chemistry & Engineering* 10 (2022): 10537–10546, https://doi.org/10.1021/acssuschemeng.2c01705.

34. H. S. Lee, K. C. Yang, S. G. Kim, et al., "SiO_2 Etch Characteristics and Environmental Impact of Ar/C_3F_6O Chemistry," *Journal of Vacuum Science & Technology, A: Vacuum, Surfaces, and Films* 36 (2018): 061306, https://doi.org/10.1116/1.5027446.

35. J. W. Hong, Y. H. Kim, H. J. Kim, et al., "Effect of Various Pulse Plasma Techniques on TiO_2 Etching for Metalens Formation," *Vacuum* 212 (2023): 111978, https://doi.org/10.1016/j.vacuum.2023.111978.

36. N. I. Cho, J. W. Hong, H. J. Yoo, et al., "Etch Characteristics of Maskless Oxide/Nitride/Oxide/Nitride (ONON) Stacked Structure Using $C_4H_2F_6$-Based Gas," *Scientific Reports* 14 (2024): 22900, https://doi.org/10.1038/s41598-024-74107-y.

37. H. J. Lee, H. W. Tak, S. B. Kim, et al., "Characteristics of High Aspect Ratio SiO_2 Etching Using $C_4H_2F_6$ Isomers," *Applied Surface Science* 639 (2023): 158190, https://doi.org/10.1016/j.apsusc.2023.158190.

38. The DUNE Collaboration, "AR6 WGI Report" (2020), https://github.com/IPCC-WG1/Chapter-7.

39. N. H. Tung, H. Lee, D. K. Dinh, et al., "Enhancing Si3N4 Selectivity Over SiO_2 in Low-RF Power NF_3–O_2 Reactive Ion Etching: The Effect of NO Surface Reaction," *Sensors (Basel, Switzerland)* 24 (2024): 3089, https://doi.org/10.3390/s24103089.

40. H. K. Lee, K. S. Chung, and J. S. Yu, "Selective Etching of Thick Si_3N_4, SiO_2 and Si by Using CF_4/O_2 and C_2F_6 Gases With or Without O_2 or Ar Addition," 2009.

41. F. Fracassi and R. D'agostino, "Contribution to Global Warming of Plasma Polymerization and Treatment Processes Fed With Fluorinated Compounds," 1999.

16128869, 2025, 10, Downloaded from https://onlinelibrary.wiley.com/doi/10.1002/ppap.70068 by Sungkyunkwan University, Wiley Online Library on [03/02/2026]. See the Terms and Conditions (https://onlinelibrary.wiley.com/terms-and-conditions) on Wiley Online Library for rules of use; OA articles are governed by the applicable Creative Commons License